Numerical study of viscous and viscoelastic fluids flow

Keslerová, Radka
Department of Technical Mathematics, Faculty of Mechanical Engineering, Czech Technical University

Kozel, Karel
Department of Technical Mathematics, Faculty of Mechanical Engineering, Czech Technical University

出版情報：Journal of Math-for-Industry (JMI). 3 (C), pp.27-32, 2012-01-27. Faculty of Mathematics, Kyushu University
バージョン：
権利関係：

Journal of Math-for-Industry, Vol. 3 (2011C-4), pp. 27–32

Numerical study of viscous and viscoelastic fluids flow

Radka Keslerová and Karel Kozel

Revised on October 24, 2011

Abstract. In this paper the numerical results for steady and unsteady flows of viscous and viscoelastic fluids are presented. The governing system of equations is based on the system of balance laws for mass and momentum for incompressible fluid. Two rheological models for the stress tensor are tested. The models used in this study are generalized Newtonian model with power-law viscosity model and Oldroyd-B model with constant viscosity. Numerical results for these models are presented.

Keywords. Navier-Stokes equations, generalized Newtonian fluids, Oldroyd-B fluids

1. Introduction

Generalized Newtonian fluids can be subdivided according to the viscosity behaviour. For Newtonian fluids the viscosity is constant and is independent of the applied shear stress (examples: water, kerosene etc). Shear thinning fluids are characterized by decreasing viscosity with increasing shear rate (ketchup, honey, blood etc). Shear thickening fluids are characterized by increasing viscosity with increasing shear rate (wet sand etc.). Figure 1 shows the dependence of shear stress and viscosity on the shear rate. For more details see e.g. [6], [9].

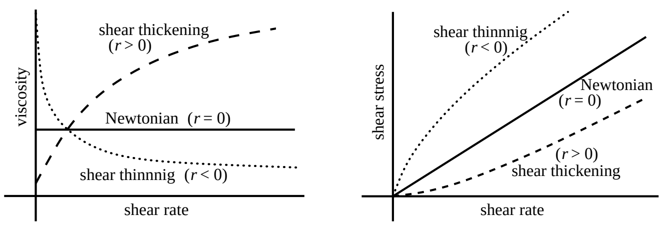

Figure 1: Viscosity and stress of generalized Newtonian fluid as a function of shear rate for power-law fluid

2. Mathematical model

The governing system of equations is the system of balance laws of mass and momentum for incompressible fluids [1], [3]:

$$\text{div } \boldsymbol{u} = 0 \tag{1}$$

$$\rho \frac{\partial \boldsymbol{u}}{\partial t} + \rho(\boldsymbol{u}.\nabla)\boldsymbol{u} = -\nabla P + \text{div } \mathbf{T} \tag{2}$$

where P is pressure, ρ is constant density, $\boldsymbol{u}$ is velocity vector. The symbol $\mathbf{T}$ represents the deviatoric stress tensor.

2.1. Stress tensor

In this work different choices of stress tensor definition are used.

a) Viscous fluids

The commonly used model corresponding to Newtonian fluid is *Newtonian model*:

$$\mathbf{T} = 2\mu\mathbf{D} \tag{3}$$

where μ is dynamic viscosity and tensor $\mathbf{D}$ is symmetric part of the velocity gradient defined by the relation (10).

This model could be generalized to take into account shear thinning and shear thickening behaviour. For this case the viscosity μ is no more constant, but is defined by viscosity function according to the power-law model [10]

$$\mu = \mu(\dot{\gamma}) = \mu_\epsilon \left(\sqrt{\text{tr}\mathbf{D}^2}\right)^r, \tag{4}$$

where μ_ϵ is a constant, e.g. the dynamic viscosity for Newtonian fluid. The symbol tr $\mathbf{D}^2$ denotes trace of the tensor $\mathbf{D}^2$. The exponent r is the power-law index. This model includes Newtonian fluids as a special case ($r = 0$). For $r > 0$ the power-law fluid is shear thickening, while for $r < 0$ it is shear thinning, (see Figure 1).

b) Viscoelastic fluids

Maxwell model is the simplest model for viscoelastic fluid. In this case the stress tensor is computed from:

$$\mathbf{T} + \lambda_1 \frac{\delta \mathbf{T}}{\delta t} = 2\mu\mathbf{D} \tag{5}$$

where λ_1 has dimension of time and denotes the *relaxation time.* The symbol $\frac{\delta}{\delta t}$ represents upper convected derivative (see eq. (9))

By combination of these two models the behaviour of mixture of viscous and viscoelastic fluids can be described.

Such a model is called *Oldroyd-B model* and it has the form

$$\mathbf{T} + \lambda_1 \frac{\delta \mathbf{T}}{\delta t} = 2\mu \left(\mathbf{D} + \lambda_2 \frac{\delta \mathbf{D}}{\delta t} \right). \tag{6}$$

The parameter λ_2 is *retardation time*, For more details see [3].

The stress tensor $\mathbf{T}$ is decomposed to the Newtonian (sometimes called solvent) part $\mathbf{T}_s$ and viscoelastic part $\mathbf{T}_e$

$$\begin{aligned} \mathbf{T} &= \mathbf{T}_s + \mathbf{T}_e, \\ \mathbf{T}_s &= 2\mu_s \mathbf{D}, \\ \mathbf{T}_e + \lambda_1 \frac{\delta \mathbf{T}_e}{\delta t} &= 2\mu_e \mathbf{D}, \end{aligned} \tag{7}$$

where

$$\frac{\lambda_2}{\lambda_1} = \frac{\mu_s}{\mu_s + \mu_e}, \qquad \mu = \mu_s + \mu_e. \tag{8}$$

The *upper convected derivative* is defined (for general tensor) by the relation (see [4])

$$\frac{\delta \mathbf{M}}{\delta t} = \frac{\partial \mathbf{M}}{\partial t} + (\boldsymbol{u}.\nabla)\mathbf{M} - \mathbf{W}\mathbf{M} + \mathbf{M}\mathbf{W} + \mathbf{D}\mathbf{M} + \mathbf{M}\mathbf{D} \tag{9}$$

where $\mathbf{D}$ is symmetric part of the velocity gradient

$$\mathbf{D} = \frac{1}{2}(\nabla \boldsymbol{u} + \nabla \boldsymbol{u}^T) = \frac{1}{2} \begin{pmatrix} 2u_x & u_y + v_x \\ u_y + v_x & v_y \end{pmatrix} \tag{10}$$

and $\mathbf{W}$ is antisymmetric part of the velocity gradient

$$\mathbf{W} = \frac{1}{2}(\nabla \boldsymbol{u} - \nabla \boldsymbol{u}^T) = \frac{1}{2} \begin{pmatrix} 0 & u_y - v_x \\ v_x - u_y & 0 \end{pmatrix}. \tag{11}$$

The governing system of equations is completed by the equation for viscoelastic part of the stress tensor

$$\frac{\partial \mathbf{T}_e}{\partial t} + (\boldsymbol{u}.\nabla)\mathbf{T}_e =$$

$$= \frac{2\mu_e}{\lambda_1}\mathbf{D} - \frac{1}{\lambda_1}\mathbf{T}_e + (\mathbf{W}\mathbf{T}_e - \mathbf{T}_e\mathbf{W}) + (\mathbf{D}\mathbf{T}_e + \mathbf{T}_e\mathbf{D}). \tag{12}$$

3. Numerical solution

3.1. Steady case

In this case the artificial compressibility method can be applied. It means that the continuity equation is completed by term $\frac{1}{\beta^2}p_t$. For more details see e.g. [2]. Let's consider Newtonian fluid model described by the system of Navier-Stokes equations in the conservative form (non-dimensional):

$$\tilde{R}W_t + F^c_x + G^c_y = \frac{1}{\mathrm{Re}}(F^v_x + G^v_y), \quad \tilde{R} = \mathrm{diag}(0,1,1). \tag{13}$$

This yields in the sense of the artificial compressibility method

$$\tilde{R}_\beta W_t + F^c_x + G^c_y = \frac{1}{\mathrm{Re}}(F^v_x + G^v_y), \tag{14}$$

$$\tilde{R}_\beta = \mathrm{diag}(\frac{1}{\beta^2}, 1, 1), \quad \beta \in \mathbb{R}^+, \tag{15}$$

where W is vector of unknowns, F^c, G^c are inviscid fluxes and F^v, G^v are viscous fluxes defined as

$$W = \begin{pmatrix} p \\ u \\ v \end{pmatrix}, \ F^c = \begin{pmatrix} u \\ u^2 + p \\ uv \end{pmatrix}, \ G^c = \begin{pmatrix} v \\ uv \\ v^2 + p \end{pmatrix}, \tag{16}$$

$$F^v = \begin{pmatrix} 0 \\ u_x \\ v_x \end{pmatrix}, \quad G^v = \begin{pmatrix} 0 \\ u_y \\ v_y \end{pmatrix} \tag{17}$$

The symbol Re denotes Reynolds number defined by the expression

$$\mathrm{Re} = \frac{\rho U L}{\mu_\epsilon}, \tag{18}$$

where U, L are reference velocity and length, μ_ϵ is dynamic Newtonian viscosity and ρ is constant density. The parameter β has dimension of a speed and denotes the artificial speed of sound. In the case of non-dimensional equations, β is then divided by a reference velocity U. This is usually an upstream velocity, which does not significantly differ from the maximum velocity in the flow field. Hence, in the case of non-dimensional equations, $\beta = 1$ is used in the presented steady numerical simulations.

Eq. (14) is discretized in space by the finite volume method (see [7]) and the arising system of ODEs is integrated in time by the explicit multistage Runge-Kutta scheme (see [5], [13]):

$$\begin{aligned} W_i^n &= W_i^{(0)} \\ W_i^{(s)} &= W_i^{(0)} - \alpha_{s-1}\Delta t \mathcal{R}(W)_i^{(s-1)} \\ W_i^{n+1} &= W_i^{(M)} \qquad\qquad s = 1, \ldots, M, \end{aligned} \tag{19}$$

where $M = 3$, $\alpha_0 = \alpha_1 = 0.5, \alpha_2 = 1.0$, the steady residual $\mathcal{R}(W)_i$ is defined by finite volume method as

$$\mathcal{R}(W)_i = \frac{1}{\sigma_i} \sum_{k=1}^{4} \left[\left(\overline{F}^c_k - \frac{1}{\mathrm{Re}} \overline{F}^v_k \right) \Delta y_k - \right. \tag{20}$$

$$\left. - \left(\overline{G}^c_k - \frac{1}{\mathrm{Re}} \overline{G}^v_k \right) \Delta x_k \right],$$

where σ_i is volume of cell, $\sigma_i = \int\int_{C_i} dx\ dy$. Symbols $\overline{F}^c_k, \overline{G}^c_k$ and $\overline{F}^v_k, \overline{G}^v_k$ denote numerical approximation of inviscid and viscous fluxes.

The inviscid numerical fluxes are computed as arithmetic average of values from two neighbouring cells

$$\overline{F}^c_k = \frac{1}{2}\left[F^c(W_i) + F^c(W_k)\right], \tag{21}$$

$$\overline{G}^c_k = \frac{1}{2}\left[G^c(W_i) + G^c(W_k)\right],$$

where index i denotes the index of the cell and index k represents index of its neighbouring cells. The mesh in the computational domain is assumed to be structured, with quadrilateral cells (see Figure 2).

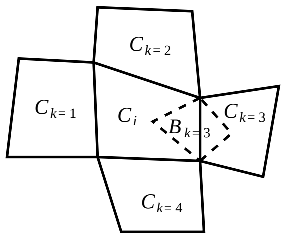

Figure 2: The structure of primary and dual control volume cell.

In the definition of viscous fluxes (17) there are partial derivatives of velocity components u, v with respect to spatial coordinates x, y. Numerical approximation of these derivatives has to be computed. Integrating these approximations over a dual cell and using Green's theorem results in (e.g. for $\overline{u}_x$)

$$\overline{u}_x \approx \frac{1}{\sigma_k} \sum_{m=1}^{4} u_m \Delta x_m, \tag{22}$$

where σ_k is volume of the dual cell corresponding to the k-th edge of the cell C_i (see Figure 2). The symbols Δx_m and Δy_m respectively are lengths of the mth-edge of the dual cell B_k in the x and y direction resp. Derivatives $\overline{u}_y, \overline{v}_x, \overline{v}_y$ are obtained in the same way.

Global behaviour of the solution during computational process is followed by the L^2 norm of the steady residual. It is given by

$$\|\mathrm{Res}(W)^n\|_{\mathrm{L}^2} = \frac{1}{num} \sqrt{\sum_i \left(\frac{W_i^{n+1} - W_i^n}{\Delta t} \right)^2} \tag{23}$$

where num is the number of the cells in the domain and $\mathrm{Res}(W)^n$ stands for a vector formed by the set of $\mathrm{Res}(W)_i^n, \forall i$. The decadic logarithm of $\|\mathrm{Res}(W)^n\|_{\mathrm{L}^2}$ is plotted in graphs presenting convergence history of simulations (see Figure 4).

3.2. Unsteady case - dual-time stepping method

The principle of dual-time stepping method is following. Artificial time τ is introduced and the artificial compressibility method in artificial time is applied. The fundamental system of equations (13) is extended to unsteady flows by adding artificial time derivatives $\partial W/\partial \tau$ to all equations, for more details see [8], [12], [5]

$$\tilde{R}_\beta W_\tau + \tilde{R} W_t + F_x^c + G_y^c = F_x^v + G_y^v \tag{24}$$

with matrices $\tilde{R}, \tilde{R}_\beta$ given by eq. (13), (15). The vector of the variables W, the inviscid fluxes F^c, G^c and the viscous fluxes F^v, G^v are given by eq. (16) and (17).

Derivatives with respect to the real time t are discretized using a three-point backward difference formula, which defines the form of unsteady residual

$$\tilde{R}_\beta \frac{W^{l+1} - W^l}{\Delta \tau} = \tag{25}$$

$$= -\tilde{R} \frac{3W^{l+1} - 4W^n + W^{n-1}}{2\Delta t} - \mathcal{R}(W)^l = -\overline{\mathcal{R}}(W)^{l+1},$$

where $\Delta t = t^{n+1} - t^n$ and $\mathcal{R}(W)$ is the steady residual defined as for steady computation, see eq. (20). The symbol $\overline{\mathcal{R}}(W)$ denotes unsteady residual. The superscript n denotes the real time index and the index l is associated with the pseudo-time. Integration in pseudo-time can be carried out by explicit multistage Runge-Kutta scheme, for more details see [11], [8].

The solution procedure is based on the assumption that the numerical solution at real time t^n is known. Setting $W_i^l = W_i^n, \forall i$, iterations in l using explicit Runge-Kutta method are performed until the condition

$$\|\overline{\mathrm{Res}}(W)^l\|_{\mathrm{L}^2} = \sqrt{\sum_i \left(\frac{W_i^{l+1} - W_i^l}{\Delta \tau} \right)^2} \leq \epsilon \tag{26}$$

is satisfied for a chosen small positive number ϵ. The symbol $\overline{\mathrm{Res}}(W)^l$ stands for the vector formed by the set of $\overline{\mathrm{Res}}(W)_i^l, \forall i$. Once the condition (26) is satisfied for a particular l, one sets $W_i^{n+1} = W_i^{l+1}, \forall i$. Then the index representing real-time level can be shifted one up. History of the convergence of unsteady residual in dual time from t^n to t^{n+1} is plotted in decadic logarithm.

4. Numerical results

In this section the numerical results are presented. Steady numerical results in the branching channel for two dimensional generalized Newtonian fluids are shown in the section 4.1. The section 4.2 is devoted to the numerical results of unsteady Newtonian fluids. In the last section 4.3 comparison of Newtonian and Oldroyd-B fluids is presented for simple 2D channel.

4.1. Two dimensional case - steady solution

In this section the steady numerical results of two dimensional incompressible laminar viscous flows for generalized Newtonian fluids are presented.

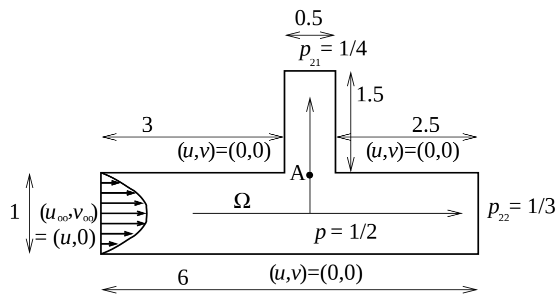

Figure 3: Initial and boundary conditions and structure of the computational domain.

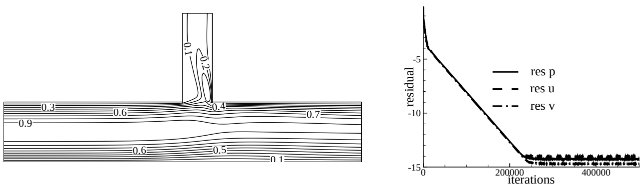

(a) Newtonian - $r = 0$

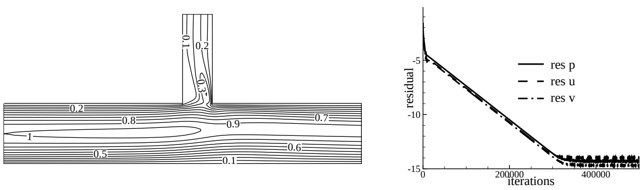

(c) shear-thickening - $r = 0.5$

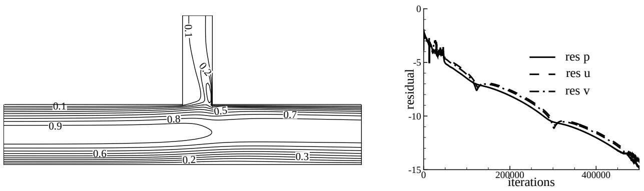

(e) shear-thinning - $r = -0.5$

Figure 4: Velocity isolines and history of the convergence of steady flows for generalized Newtonian fluids.

The following choices of the power-law index were used. For Newtonian fluid $r = 0$, for shear thickening and shear thinning fluid values $r = 0.5$ (shear thickening) and $r = -0.5$ (shear thinning) are used. The flow is computed in the branching channel with Reynolds number Re $= 400$ where the steady boundary condition shown in Figure 3 are used.

In Figure 3 the initial conditions are sketched. In the inlet the velocity is prescribed by the parabolic profile. In Figure 4 velocity isolines and histories of the convergence are presented. One of the main differences between Newtonian and non-Newtonian fluids flow is in the size of the separation region. This is in the place where the channel is branched. From Figures 4 and 5, the separation region is the smallest for shear thickening fluids and the biggest separation region is for the shear thinning fluids.

In Figure 6 nondimensional axial velocity profile for steady fully developed flow of Newtonian, shear thickening and shear thinning fluids is shown. In these figures the small channel is sketched. The line (inside the domain) marks the position where the cuts for the velocity profile were done.

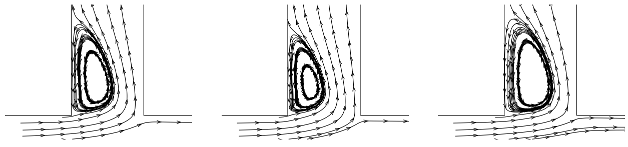

(a) Newtonian (b) shear-thickening (c) shear-thinning

Figure 5: Separation region for generalized Newtonian fluids.

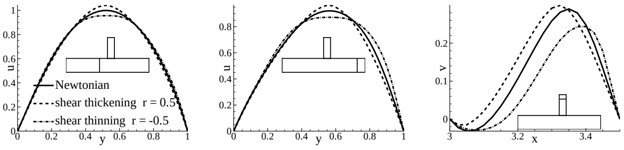

(a) (b) (c)

Figure 6: Nondimensional velocity profile for steady fully developed flow of generalized Newtonian fluids in the branching channel (the line legend in the a) is the same for all figures).

4.2. Two dimensional - unsteady case

In this section two dimensional numerical results for Newtonian unsteady flow through the branching channel are presented. The dual-time stepping method is used. The unsteady boundary conditions were considered, see Figure 3. In the branch (going up) the pressure is prescribed by pressure function

$$p_{21} = \frac{1}{4}\left(1 + \frac{1}{2}sin(\omega t)\right), \quad \omega = 2\pi f, \quad f = 2. \qquad (27)$$

In Figure 7 graphs of pressure $p_{21}(t)$ and velocity in the point A (see Figure 3) are shown. The square symbols mark positions in time of the snapshots shown in Figure 8 during one period.

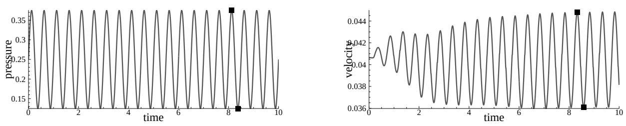

(a) pressure (b) velocity

Figure 7: The graphs of the pressure and the velocity as the function of the time.

As initial data the numerical solution of steady fully developed flow of Newtonian fluid in the branching channel was used. The artificial compressibility coefficient β was chosen 10 in this case. Reynolds number is 400.

In Figure 8 unsteady numerical results during one period are presented. In Figure 9 the decadic logarithm of the L^2 norm of unsteady residual is shown.

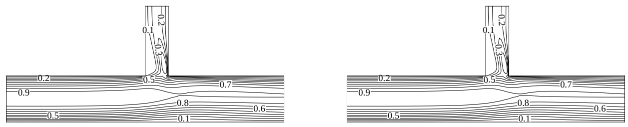

(a) $t = 8.3$ (b) $t = 8.6$

Figure 8: Velocity isolines of unsteady flow of Newtonian fluids.

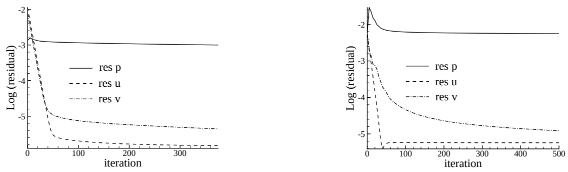

(a) $t = 8.3$ (b) $t = 8.6$

Figure 9: The L^2 norm of the unsteady residual.

4.3. Oldroyd-B model

In this section the comparison of the numerical simulations of Newtonian and Oldroyd-B fluids are presented. In Figure 10 the shape of the tested domain is sketched.

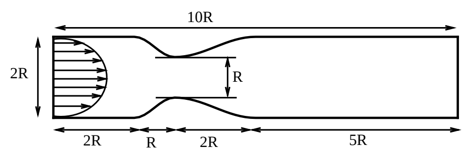

Figure 10: Structure of the computational domain.

The following model parameters are used:

$$\mu_e = 4.0 \cdot 10^{-4} Pa \cdot s \qquad \mu_s = 3.6 \cdot 10^{-3} Pa \cdot s$$
$$\lambda_1 = 0.06s \qquad \lambda_2 = 0.054s$$
$$U_0 = 0.0615 m \cdot s^{-1} \qquad L_0 = 2R = 0.0062m$$
$$\mu_0 = \mu = \mu_s + \mu_e \qquad \rho = 1050 kg \cdot m^{-3}$$
$$\mathrm{Re} = \frac{\rho U L}{\mu_0}$$

Figures 11 and 12 show the comparison of axial velocity isolines and pressure distributions.

In Figure 13 the separation region for both tested fluids flow is shown.

Figure 14 presents this comparison in the pressure and the velocity distribution through the tested domain.

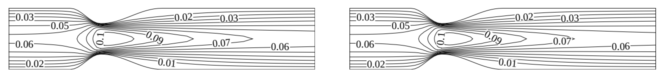

(a) Newtonian (b) Oldroyd-B

Figure 11: Axial velocity isolines for Newtonian and Oldroyd-B fluids.

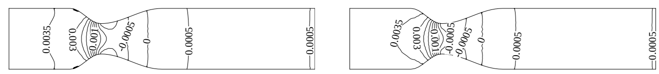

(a) Newtonian (b) Oldroyd-B

Figure 12: Pressure distribution for Newtonian and Oldroyd-B fluids.

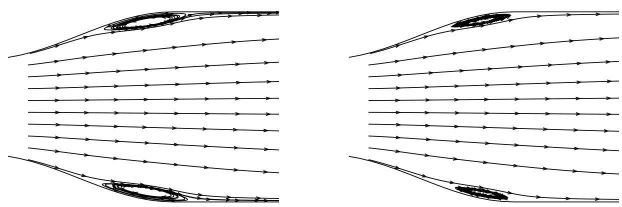

(a) Newtonian (b) Oldroyd-B

Figure 13: Streamlines for Newtonian and Oldroyd-B fluids.

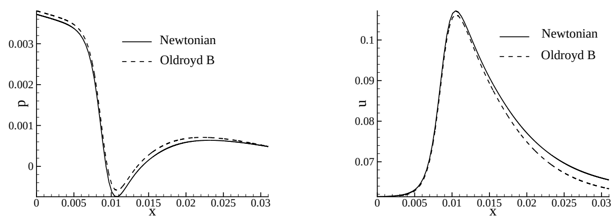

(a) pressure (b) axial velocity

Figure 14: Pressure and axial velocity distribution along the central axis of the channel.

5. Conclusions

In this paper a finite volume solver for incompressible laminar viscous and viscoelastic flows in the branching channel was described. Two classes of fluids (viscous and viscoelastic) were considered. The corresponding mathematical models (Newtonian and Oldroyd-B) were used for testing. Generalized Newtonian model was used for numerical modelling of Newtonian and some non-Newtonian fluids flow. The numerical results obtained by this method were presented. For the generalized Newtonian fluids the power-law model was used.

The numerical results of Oldroyd-B model were compared with the numerical results of Newtonian mathematical model (assumption of constant viscosity).

The explicit Runge-Kutta method was considered for numerical modelling. The convergence history confirms robustness of the applied method. The dual-time stepping method was used for unsteady numerical modelling of Newtonian fluids flow.

Acknowledgment

This work was partly supported by the grant GACR P201/11/1304 and GACR 201/09/0917, Research Plan MSM 684 077 0003 and Research Plan MSM 684 077 0010.

References

[1] R. Dvořák and K. Kozel: *Mathematical Modelling in Aerodynamics (in Czech)*. CTU, Prague, Czech Republic, 1996.

[2] A.J. Chorin, A numerical method for solving incompressible viscous flow problem, *Journal of Computational Physics* **135** (1967) 118–125.

[3] T. Bodnar and A. Sequeira and M. Prosi, On the shear-thinning and viscoelastic effects of blood flow under various flow rates, *Applied Mathematics and Computation* (2010).

[4] T. Bodnar and A. Sequeira, Numerical Study of the Significance of the Non-Newtonian Nature of Blood in Steady Flow through s Stenosed Vessel (Editor: R. Ranacher, A. Sequeira), *Advances in Mathematical Fluid Mechanics* (2010) 83–104.

[5] R. Keslerová and K. Kozel, Numerical Simulations of Incompressible Laminar Flow for Newtonian and Non-Newtonian Fluids (Editor: K. Kunisch, G. Of, O. Steinbach), *Numerical Mathematics and Advanced Applications, ENUMATH 2007* (2008) 465–472.

[6] R.P. Chhabra and J.F. Richardson: *Non-Newtonian Flow in the Process Industries*. Biddles Ltd, Guildford and King's Lynn, Great Britain, 1999.

[7] R. LeVeque: *Finite-Volume Methods for Hyperbolic Problems*. Cambridge University Press, 2004.

[8] A.L. Gaitonde, A Dual-Time Method for Two Dimensional Unsteady Incompressible Flow Calculations, *International Journal for Numerical Methods in Engineering* **41** (1998) 1153–1166.

[9] A.M. Robertson and A. Sequeira and M.V. Kameneva: *Hemorheology*. Birkhäuser Verlag Basel, Switzerland, 2008.

[10] A.M. Robertson: *Review of Relevant Continuum Mechanics*. Birkhäuser Verlag Basel, Switzerland, 2008.

[11] R. Honzátko, *Numerical Simulations of Incompressible Flows with Dynamical and Aeroelastic Effects*. PhD thesis, Czech Technical University, Prague, Czech Republic, 2007.

[12] D. Mateescu and M.P. Païdoussis and F. Bélanger, A Time-Integration Method Using Artificial Compressibility for Unsteady Viscous Flows, *Journal of Sound and Vibration* **177(2)** (1994) 197–205.

[13] J. Vimmr and A.Jonášová, Non-Newtonian Effects of Blood Flow in Complete Coronary and Femoral Bypasses, *Mathematics and Computers in Simulation* **80** (2010) 1324–1336.

Radka Keslerová and Karel Kozel
Department of Technical Mathematics, Faculty of Mechanical Engineering, Czech Technical University, Karlovo nam. 13, 121 35 Prague, Czech Republic
E-mail: keslerov(at)marian.fsik.cvut.cz
karel.kozel(at)fs.cvut.cz